An Observational and Theoretical Study of Atmospheric Flow Over a Heated Island: Part II[1]

CHANDRAKANT M. BHUMRALKAR [2]—*Department of Geophysical Sciences,*
Old Dominion University, Norfolk, Va.

ABSTRACT—A two-dimensional theoretical model is developed to analyze the properties of perturbations induced when air flows over an isolated warm portion of the earth's surface. The model equations include continuity equations that predict water vapor, cloud water, and liquid water. The nonadiabatic effects of condensational heating and evaporational cooling are also incorporated.

The theoretical model is developed in conjunction with a specially designed observational field program for testing the model predictions. The field program and its results are described in Part I.

The model has been able to reproduce the observed conditions quite realistically; in particular, the observed and predicted patterns of cloud distributions and rainfall compare very well. The study has demonstrated the important influence of evaporational cooling of the environment on the behavior of perturbations induced by the heat source.

Numerical integrations of the model have also been performed to examine the dependence of the induced perturbations on the following factors: (1) temperature excess of the heat source, (2) speed of the normal component of the prevailing flow, (3) speed of the parallel component of the prevailing flow, and (4) width of the heat source. The results show that the larger the temperature excess of the heat source, the greater the intensity of the induced disturbance. The strength of the normal and the parallel components of the prevailing flow have opposite influences on the perturbations—a stronger normal component tends to weaken the disturbance whereas a stronger parallel component tends to intensify it.

1. INTRODUCTION

As we explained in the introduction to Part I (Bhumralkar 1973), the objective of this part of our two-part study is

1. To develop a general, theoretical, nonlinear model that can analyze the properties of perturbations induced when air flows over a heated island; and
2. to test the results of the model by comparing these properties with actual observations collected on the space and time scale of the perturbations induced by the heated island.

The observational field program and its results have been discussed in detail in Part I.

2. THE PHYSICAL MODEL

A two-dimensional cross-section model is considered; thus, physically the solutions apply to a heated island of infinite length. The consideration of a two-dimensional model appears to be valid for our study since we wish to apply it to the real Grand Bahama Island, which has essentially two-dimensional features.

The atmosphere is modeled as consisting of two layers. The lower layer is the constant-flux layer, and its top is arbitrarily set at 25 m. The second layer, extending to 12

km in height, is the region within which the actual time integrations are carried out.

Our model assumes that the atmosphere is always in hydrostatic balance. The physical model also includes the penetrative convection mixing through parameterized formulations based on the theory described by Estoque (1968). The details of the formulations are given by Bhumralkar (1972).

The dynamic and thermodynamic influences of the phase change of water substance have been included following the procedure given by Kessler (1969). The model also simulates evaporational cooling at the lower boundary when sufficient rain water reaches the ground. However, we have not considered the cloud shadow effect on the surface temperature because the observations show that this effect is much smaller than the evaporational cooling from the surface rain.

The effect of the liquid water within clouds, in terms of the actual weight of the water as it affects buoyancy, has been incorporated by suitably modifying the hydrostatic equation.

3. DYNAMIC EQUATIONS

The equations have been formulated in Cartesian coordinates (fig. 1). The origin is located at the midpoint of an island that is infinitely long in the y direction. This assumption implies that there is horizontal homogeneity of motion, temperature, and moisture in this direction.
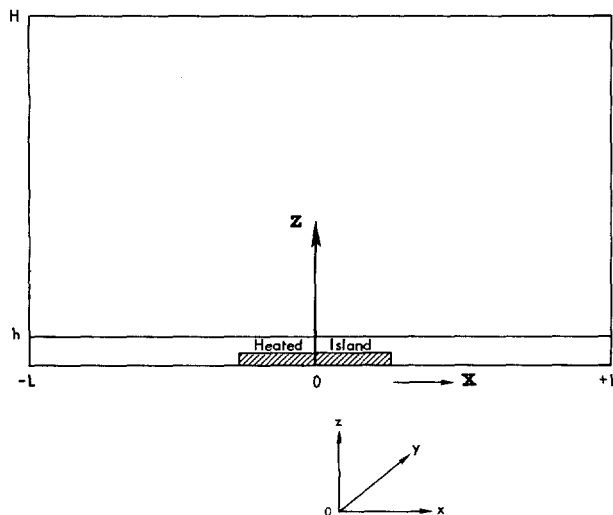
FIGURE 1.—The coordinate system.

We may thus write the horizontal equations of motion as

$$\frac{\partial u}{\partial t}=-u\frac{\partial u}{\partial x}-w\frac{\partial u}{\partial z}+fv-\frac{1}{\rho_s}\frac{\partial p}{\partial x}+\frac{\partial}{\partial z}\left(K_z\frac{\partial u}{\partial z}\right)+K_x\frac{\partial^2 u}{\partial x^2} \quad (1)$$

and

$$\frac{\partial v}{\partial t}=-u\frac{\partial v}{\partial x}-w\frac{\partial v}{\partial z}+f(u_g-u)+\frac{\partial}{\partial z}\left(K_z\frac{\partial v}{\partial z}\right)+K_x\frac{\partial^2 v}{\partial x^2}. \quad (2)$$

In accordance with our physical model, the vertical equation of motion (i.e., the hydrostatic equation) can be written as:

$$\frac{\partial}{\partial z}\left(\frac{p}{p_0}\right)^\kappa=\frac{g}{c_p\theta}\left(\frac{1}{1+\Delta\theta}\right) \quad (3)$$

where $\Delta\theta$ incorporates the effect of moisture, in vapor and liquid forms, on the hydrostatic pressure. An expression for $\Delta\theta$ in terms of Q, Q_R, has been derived by Bhumralkar (1974).

The continuity equation for mass is

$$\frac{\partial}{\partial x}(\rho_s u)+\frac{\partial}{\partial z}(\rho_s w)=0. \quad (4)$$

The equation of state is

$$p=\rho RT \quad (5)$$

where $T=\theta(p/p_0)^\kappa$.

The variables are in customary notation. The geostrophic wind component, u_g in eq (2), is proportional to the synoptic scale pressure gradient force in the y direction. In our computations, this wind is prescribed as an arbitrary function of height and is invariant in time. The term ρ_s represents the value of density for the standard atmosphere. The last two terms on the right sides of eq (1) and (2) represent, respectively, the vertical and horizontal subgrid, small-scale eddy diffusion processes. Analogous terms also appear in the moisture equation [eq (6)] and the thermodynamical equation [eq (8)].

Equations (1) and (2) apply to the atmosphere above the constant-flux layer. The profiles of wind, temperature, and moisture within this constant flux layer have been computed by using the equations described by Estoque and Bhumralkar (1969).

4. MOISTURE EQUATIONS

We do not consider the ice phase in our model. The equations for water follow the formulations described by Kessler (1969) in which he uses the parameterization approach to the modeling of cloud microphysical processes. The following processes are incorporated in the moisture equations:

1. Condensation of water vapor into clouds in rising saturated air and evaporation of clouds in descending air.
2. Autoconversion or coalescence of cloud droplets *into* precipitation drops.
3. Accretion or collection of cloud droplets *by* the larger precipitation drops.
4. Evaporation of precipitation in unsaturated air.
5. Transport of cloud and precipitation by air motions and the settling of precipitation.

Thus, the conservation equations for water vapor *plus* cloud water and rain water are

$$\frac{\partial Q}{\partial t}=-u\frac{\partial Q}{\partial x}-w\frac{\partial Q}{\partial z}+\frac{\partial}{\partial z}\left(K_z\frac{\partial Q}{\partial z}\right)+K_x\frac{\partial^2 Q}{\partial x^2}+\text{CON}Q$$
$$-\text{AUCON }(Q\rightarrow Q_R)-\text{ACR }(Q\rightarrow Q_R)$$
$$+\text{EVAP }(Q_R\rightarrow Q) \quad (6)$$

and

$$\frac{\partial Q_R}{\partial t}=-u\frac{\partial Q_R}{\partial x}-w\frac{\partial Q_R}{\partial z}-\frac{1}{\rho_s}\frac{\partial}{\partial z}(\rho_s V_R Q_R)$$
$$+\text{AUCON }(Q\rightarrow Q_R)+\text{ACR }(Q\rightarrow Q_R)$$
$$-\text{EVAP }(Q_R\rightarrow Q). \quad (7)$$

The third and fourth terms in eq (6) represent subgrid-scale Fickian-type diffusion processes for Q. The fifth term, $\text{CON}Q$, represents vertical mixing of moisture due to penetrative convection. We do not consider any subgrid-scale transport processes for rain water, Q_R. The arrows in the different cloud microphysical and precipitation terms indicate the direction of conversion of one form into another. Formulations for autoconversion, accretion, and evaporation are defined as follows:

$$\text{AUCON}=k_1[\rho_s(Q-q_s)-k_2]$$

where k_1 and k_2 are empirical constants such that

$$k_1\begin{cases}>0 & \text{for } \rho_s(Q-q_s)>k_2,\\ =0 & \text{for } \rho_s(Q-q_s)<k_2,\end{cases}$$

$$\text{ACR}=k_3\rho_s(Q-q_s)(\rho_s Q_R\cdot 10^6)^{0.875}$$

where

$$k_3\begin{cases}>0 & \text{for } Q>q_s \text{ and } Q_R>0,\\ =0 & \text{for } Q<q_s,\end{cases}$$

and

$$\text{EVAP}=k_4\rho_s(q_s-Q)(\rho_s Q_R\cdot 10^6)^{0.65}$$

where

$$k_4\begin{cases}>0 & \text{for } Q<q_s \text{ and } Q_R>0,\\ =0 & \text{for } Q>q_s.\end{cases}$$

A more detailed discussion of the above formulations is given by Kessler (1969).

The preceding moisture equations assume that liquid water may exist in two forms, cloud water ($Q_c = Q - q_s$) and rain water (Q_R). Furthermore, we also assume that cloud water is transported by the wind without any relative motion. Rain water, on the other hand, is allowed to have a relative fall velocity (V_R), which is considered to be the same for all particles comprising precipitation at a particular time and height. It can be noted from the above expressions that the empirical constants control the various microphysical processes. For example, the partition of condensed water substance into cloud water or rain water depends upon k_1, k_2, and k_3. For our computations, we have used exactly the same values for the constants as those used by Kessler (1969). However, it is evident that these need to be assessed properly under varying conditions.

5. THERMODYNAMICAL EQUATION

The thermodynamic energy equation may be written in the form

$$\frac{\partial\theta}{\partial t} = -u\frac{\partial\theta}{\partial x} - w\frac{\partial\theta}{\partial z} + \frac{\partial}{\partial z}\left(K_z\frac{\partial\theta}{\partial z}\right) + K_x\frac{\partial^2\theta}{\partial x^2} + \text{CON }\theta$$
$$+ \frac{\theta}{c_p T}(S_1 + S_2) + \frac{\theta}{c_p T}S_3. \quad (8)$$

The third and fourth terms in eq (8) represent subgrid, small-scale eddy transport processes. The fifth term, CONθ, represents vertical mixing of heat due to cumulus-scale processes. This term is formulated in the same way as the analogous term CONQ in eq (6). The values $(S_1 + S_2)$ and S_3 are the nonadiabatic contributions to the changes in θ. The most important contribution is that of S_1, which evaluates the latent heat released or consumed when the water substance changes phase. Thus,

$$S_1 = k_5\left(-L\frac{dq_s}{dt}\right) \quad (9)$$

where

$$k_5\begin{cases} =1 & \text{for } Q \geq q_s \\ =0 & \text{for } Q < q_s \end{cases}$$

and

$$\frac{dq_s}{dt} = -\frac{g}{R}\left(\frac{\epsilon L - c_p T}{c_p T^2 + \frac{L^2 q_s}{R_V}}\right)q_s w.$$

From the preceding expressions, it can be easily verified that under supersaturated conditions, S_1 is a source of θ for upward motions and a sink for downward motions.

Also,

$$S_2 = k_5\left(LK_x\frac{\partial^2 Q}{\partial x^2}\right)$$

where

$$k_5\begin{cases} =1 & \text{for } Q \geq q_s \\ =0 & \text{for } Q < q_s \end{cases}$$

$$S_3 = -k_6 L\frac{dQ_R}{dt}$$

TABLE 1.—*Grid Spacing: Height z above the surface for the height index J, and distance x from the center of the heated island for the horizontal index I*

J	z (m)	I	x (km)	I	x (km)
1	0.0	1	−500.0	17	1.0
2	10	2	−220.0	18	2.0
3	25	3	−110.0	19	3.0
4	225	4	−65.0	20	4.0
5	425	5	−38.0	21	5.0
6	650	6	−24.0	22	6.0
7	900	7	−15.0	23	8.0
8	1200	8	−10.0	24	10.0
9	1550	9	−8.0	25	15.0
10	1950	10	−6.0	26	20.0
11	2450	11	−5.0	27	30.0
12	3100	12	−4.0	28	45.0
13	3900	13	−3.0	29	60.0
14	4900	14	−2.0	30	80.0
15	6300	15	−1.0	31	100.0
16	8500	16	0.0		
17	12000				

where

$$k_6\begin{cases} =0 & \text{for } Q \geq q_s \\ =1 & \text{for } Q < q_s \end{cases},$$

and

$$\frac{dQ_R}{dt} = k_4\rho_s(q_s - Q)(\rho_s Q_R \cdot 10^6)^{0.65}.$$

In summary, the nonadiabatic feedback effects due to change in phase of water substance are incorporated as follows:

1. For upward saturated motions, heat is released due to condensation (source).
2. For downward saturated motions, heat is consumed due to evaporation (sink).
3. When rain water reaches unsaturated air, there is cooling due to evaporation (sink).

6. NUMERICAL METHOD

The Grid and the Domain

We use a Cartesian grid consisting of 31 points along the x direction and 17 points along z. The y axis is oriented parallel to the longer axis of the heated island and x axis perpendicular to it. The variable grid spacing (table 1) is designed in such a way that we obtain a higher resolution at lower levels and in the vicinity of the heated island. From this region of prime interest, the grid spacing is incremented outward to the two lateral boundaries and upward to the top boundary. The upwind and downwind lateral boundaries of the domain of integration are located at $x = -500$ km and $x = 100$ km, respectively. The lower and upper boundaries are located respectively at the surface ($z = 0$) and 12 km. The heated island is specified by prescribing a higher temperature, lower relative humidity, and greater roughness parameter over a 10 km-wide portion of the lower boundary, $z = 0$, with the origin of the coordinate system coinciding with the center of the island.

Initial Conditions

The experiments were designed to study the response of the atmospheric flow over a heated island, and we treat this as an initial value problem. In our primitive-equation model, the wind is assumed to be in geostrophic equilibrium at the initial time. The corresponding temperature field is computed from the wind field using the thermal wind relations. It is evident that the initial balanced state may be assumed to represent the prevailing synoptic-scale conditions, and any subsequent deviations from the initial field represent mesoscale motions associated with the differential heating and frictional influences only.

We include friction typical of the island surface. The Coriolis parameter, f, corresponding to the latitude (26.5°N) of Grand Bahama Island, is assumed constant over the entire domain of integration. We use tropical standard atmosphere values for the basic state density field, which is allowed to vary only with height.

Boundary Conditions

At the upper boundary, $z=H$, we allow the pressure to vary, in time, through dynamic considerations. The physical assumption is that there is a rigid lid at $z=H$. The fluid pushes against the lid to set up a pressure gradient along it. This pressure distribution is calculated by assuming that the horizontal flux across $0 \leq z \leq H$ is zero, apart from the geostrophically balanced synoptic flow. A detailed description of the method is given by Bhumralkar (1972). In practice, we need to prescribe the pressure only at the top of the lateral boundary $x = -500$ km.

At the lower boundary ($z=0$), we prescribe no-slip conditions on velocity so that $u=v=0$ and also $w=0$ (flat topography). The potential temperature at the surface can be prescribed as

$$\theta = 300°K \qquad \text{for } -L \leq x < -5 \text{ km}$$
$$\theta = 306°K \qquad \text{for } -5 \text{ km} \leq x \leq 5 \text{ km}$$
$$\theta = 300°K \qquad \text{for } 5 \text{ km} < x \leq L.$$

Whenever the ground is wet due to sufficient rain reaching the surface, θ at the island surface is allowed to decrease and the mixing ratio is allowed to attain the saturation value corresponding to the new θ. The method of effecting the evaporational cooling of the island surface temperature due to rain is described by Bhumralkar (1972).

The lateral boundary conditions are such that at the inflow points the dependent variables are assumed to be uniform along x; at the outflow points the differencing scheme does not require boundary values of these variables.

Diffusion Coefficients

We prescribe a constant value of 200 m²/s for the vertical diffusion coefficient, K_z. This may be compared with the values of 500 m²/s (Takeda 1971) and 80 m²/s (Orville and Sloan 1970). The horizontal diffusion coefficient K_x is obtained, following Richardson (Sutton 1953, p. 320),

Table 2.—*Summary of numerical experiments*

Experiment No.	Island temperature excess (°C)	Wind direction (°)/speed (m/s)	Component normal to is. (m/s)	Component parallel to is. (m/s)	Width (km)	Comparison with observations feasible?
1 Control	6	155/5	2.0	4.6	10	Yes (Aug. 27 1970)
2	6	155/12	4.8	11.0	10	Yes (Aug. 28 1970)
3	9	155/5	2.0	4.6	10	No
4	3	155/5	2.0	4.6	10	No
5	6	155/5	2.0	10.0	10	No
6	6	155/5	2.0	4.6	4	No
7	6	155/5	2.0	4.6	2	No

from

$$K_x = \beta(\Delta x)^{4/3}$$

where β is a proportionality constant and Δx is the horizontal grid mesh size.

Finite-Difference Scheme

We integrate the model equations by using the semi-implicit version of the forward-upstream differencing scheme (Richtmyer 1957). The time interval of integration is 20 s.

7. RESULTS OF THE NUMERICAL EXPERIMENTS

We performed *seven* integrations of our model using the numerical techniques and the boundary and the initial conditions described in section 6. Table 2 summarizes the main features of these experiments. We designate experiment 1 as the control experiment for the purpose of simulating the atmospheric conditions of Aug. 27, 1970, over and in the vicinity of Grand Bahama Island (GBI). The selection of this particular date is based on the consideration that, as shown by observational results in Part I, the heated island effect is most pronounced on August 27, and we have sufficient information for a qualitative verification of the model predictions. The initial conditions used in experiment 2 differ from the control experiment only in the speed of the prevailing flow; thus, experiment 2 simulates the conditions of Aug. 28, 1970. Experiments 3 to 7 enable us to isolate and analyze the dependence of perturbations, induced by a heated island, on factors such as the intensity of the wind component parallel to the island, the temperature excess of the heat source, and the width of the island. Unlike experiments 1 and 2, however, there is no direct verification of the results of experiments 3 to 7 by actual observations.

Experiment 1: The Control Experiment

The structural properties of the prevailing atmospheric conditions on Aug. 27, 1970, are incorporated by using appropriate initial and boundary conditions. The initial

wind, without shear, is 155° and 5 m/s. This implies that, for our experiment, the components of wind normal to and along the island are respectively 2 and 4.6 m/s. The initial distributions of θ and Q are horizontally uniform at all levels. At the lower boundary, the island is prescribed to be warmer and drier than the surrounding sea. Thus, for experiment 1 the boundary conditions at the surface are as follows:

1. $u=v=0$,
2. sea-surface potential temperature $=300°$K,
3. island potential temperature $=306°$K,
4. mixing ratio at the sea surface $=23.8$ g/kg, and
5. mixing ratio at the island surface $=18.5$ g/kg.

We integrated the model for 4 hr of real time. This duration is found to be adequate for simulating a disturbance induced by the heated island.

It may be noted that we have used a single-step function to specify the island-heating for starting our integrations. The island surface temperature is allowed to remain constant unless rainfall reaches the surface, when cooling due to evaporation is effected according to a parameterized approximation described by Bhumralkar (1972). We used this technique, instead of using a time-dependent heating function, essentially for want of sufficient computer time. For the same reason, only the daytime influence of the heated island was simulated. Thus, the integrations purport to simulate the atmospheric conditions over and in the vicinity of the island for the daytime period starting from 1300 Eastern Daylight Time (EDT).

At the initial time, there are no perturbations in any of the fields; the rainfall is zero over the entire domain. As the integration proceeds, perturbations develop over the island in response to the surface heating and friction.

In this section, we describe the evolution of the disturbance through its entire life cycle. In all our subsequent discussions, the terms "leeward," "downwind," and "upwind" pertain to the initial normal component of the prevailing wind. Also, the perturbations of any quantity are the deviations from its value at the upwind boundary. All references to temperature imply potential temperature.

Figures 2–7 indicate the development of the perturbations with time. These show the two-dimensional fields of wind velocity in the x, z plane, vertical velocity, w, and temperature, θ', at $t=1.5$, 1.75, 2.0, 2.25, 2.75, and 3 hr after the initial time. The cross-hatched areas superposed on wind and θ' fields represent saturated areas; rainy areas have also been marked on θ' fields.

In the earlier stages of the integration, two separate circulation cells (not shown), one over each edge of the heated island, develop in response to the strong solenoidal field at these two locations. As time progresses, these cells coalesce into one organized cell which, at $t=1.5$ hr, is located at the leeward edge of the island (fig. 2). With this organization of the updraft, the cloud, which first appears at $t=1.5$ hr, grows, and the maximum cloud water content attained is 0.8 g/kg. The latent heat of condensation is released, which in turn further intensifies

the updraft. The maximum vertical velocity at $t=1.75$ hr is 6 m/s. Precipitation in the form of liquid water descends to unsaturated levels and causes evaporational cooling of the environment.

During the next 15 min, the main updraft drifts downwind and reaches a location over the sea (fig. 3), and the absence of a heat source there causes it to decrease in intensity to approximately 3 m/s. Also, another updraft ($\sim$ 1 m/s) forms over the island. The most noteworthy feature at this time is the strong compensating downdraft (2.6 m/s), which probably forms as a result of the weight of water and evaporational cooling. The cloud is depleted of its liquid water content and decreases in size; the cloud-water amount decreases from 0.8 to 0.2 g/kg. The evaporational cooling below the cloud and within the rain area becomes more extensive.

After we integrate the model for 2.25 hr of real time, the vertical circulation cell off the island moves further downwind and weakens appreciably (fig. 4). However, the updraft over the island intensifies and narrows considerably. The maximum vertical velocity of 12 m/s occurs for a short duration only and there is a distinct shift of the disturbance in the upwind direction. The rainfall reaches and cools the surface. Also, the cooling of environmental air in lower levels, though still confined to the downwind side of the island, becomes quite widespread.

It is important to note that at this time the low-level flow in the x, z plane *reverses* itself and is now moving from the leeward to the upwind edge of the island. This apparent propagation of the disturbance (in the upwind direction) is caused by evaporational cooling. It is our hypothesis that a mesoscale High forms near the leeward edge of the island in response to the evaporational cooling of the ambient atmosphere as well as the island surface. This high in turn accelerates the air in the upwind direction. This is clearly indicated by figure 5, which shows an x, t cross section of the surface pressure perturbation. Note that, in the earlier stages, the island heating creates relatively lower pressure over the island. Note also the formation of a mesoscale Low at the lee edge at $t=1.75$ hr in response to condensational heating. After $t=1.75$ hr, evaporational cooling becomes predominant and a meso-High develops at about $t=2.25$ hr. This high persists until almost the end of the integration.

Figure 6 shows that the updraft continues its movement in the upwind direction and weakens in intensity. The maximum vertical velocity at $t=2.5$ hr and 2.75 hr is, respectively, 8.5 and 2 m/s. The cloudiness appears to extend itself over the entire width of the island. Beyond this time, however, the upward motions have almost moved off to the upwind side of the island. In the lower levels over the island, there is a general weak downward motion. The region of negative θ' increases and the warming in upper levels decreases.

After the integration proceeds for 3 hr or more of real time, the disturbance, as indicated by vertical velocity and cloudiness, almost subsides (fig. 7). At $t=3$ hr, the island surface cools across its entire width and there is widespread
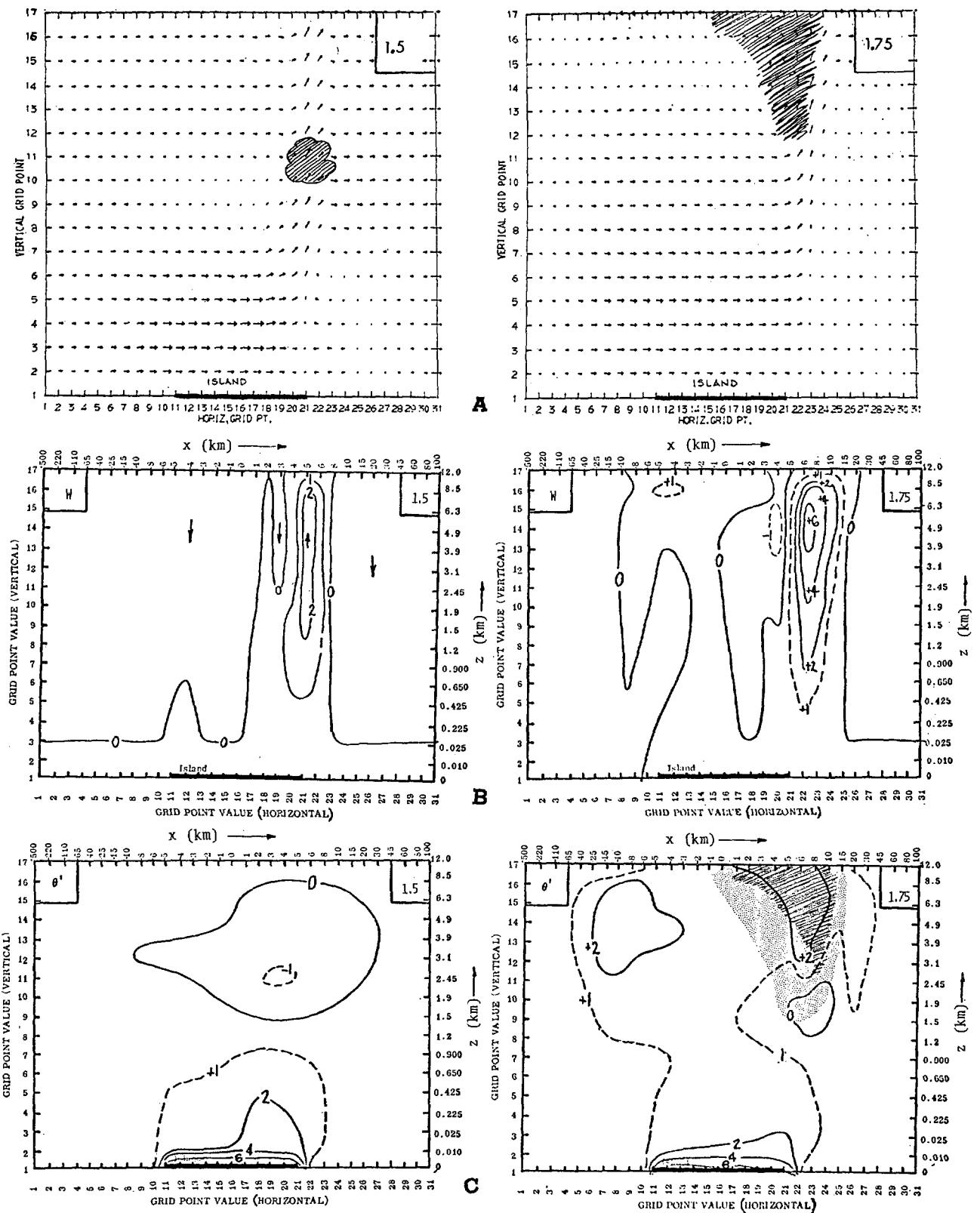
FIGURE 2.—Theoretical distributions of (A) wind velocity in the x, z plane (m/s), (B) vertical velocity (m/s), and (C) perturbation potential temperature (°C) at 1.5 and 1.75 hr of real time. Cross-hatched portions represent saturated regions; screen shows the rain area.

cooling of the atmosphere in the vicinity of the island; downward motions predominate over the entire island.

Comparison: Model Predictions Versus Observations

The ultimate test of the validity of a model is the degree

of correspondence between its predictions and reality. We now present a qualitative comparison between the theoretical results and a real atmospheric situation.

Theoretical results. Figure 8 shows an x, t cross section of the theoretical rainfall rate (cm/15 min) at the surface of the island. This cross section covers the entire duration
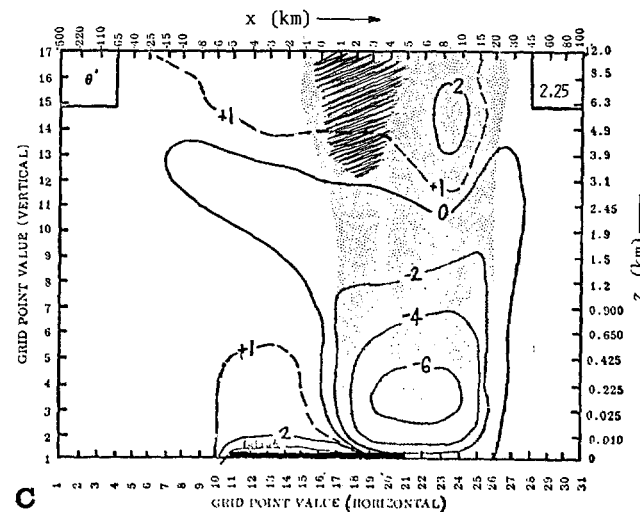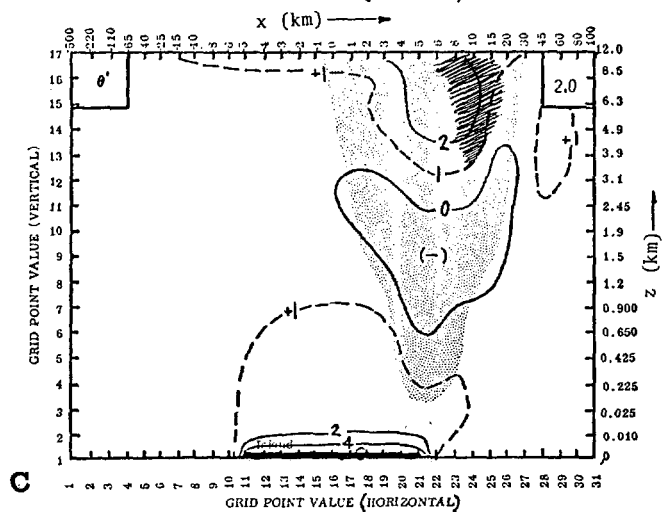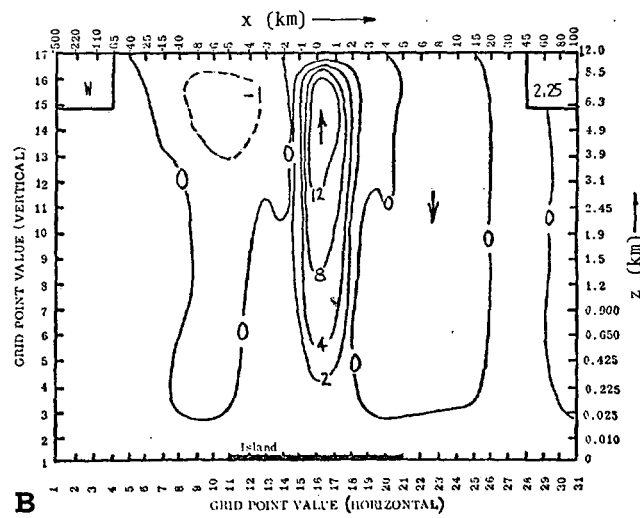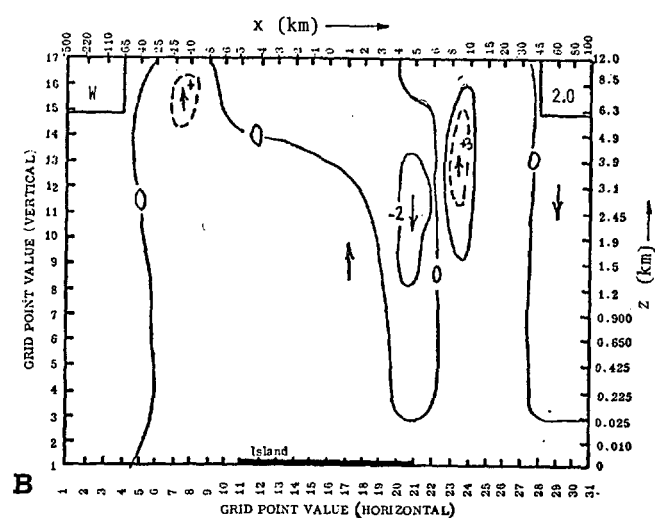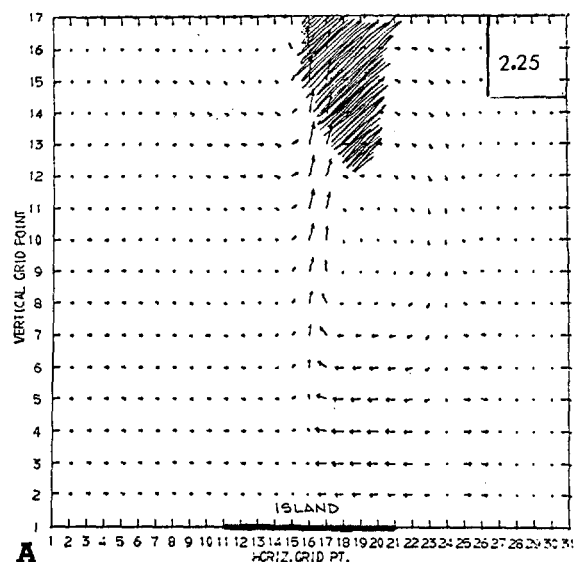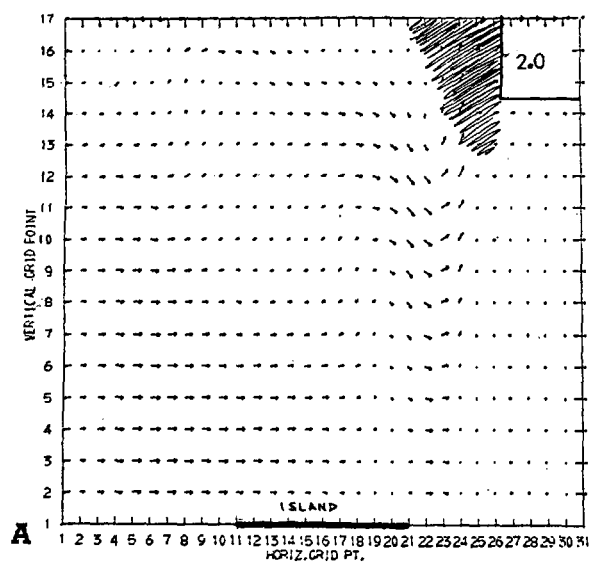
FIGURE 3.—Same as figure 2 for 2.0 hr.

FIGURE 4.—Same as figure 2 for 2.25 hr.

of numerical integration of the model. The following features are evident from this figure.

In the initial stages of the computations, there is no significant rain reaching the surface of the island. After a lapse of 1.5 and 1.75 hr from the initial time, however, there is sudden onset of rain confined to the leeward edge of the island. During the next hour, the maxima of rainfall

rate moves in the upwind direction and is located over the major portion of the island; rain reaches the ground and covers the entire width of the island. At $t=3.5$ hr, there is very little precipitation at the surface, implying thereby that the disturbance has weakened considerably. Finally, the life cycle of this particular disturbance (as shown by rainfall rate at the surface) is about 2 to 2.5 hr.
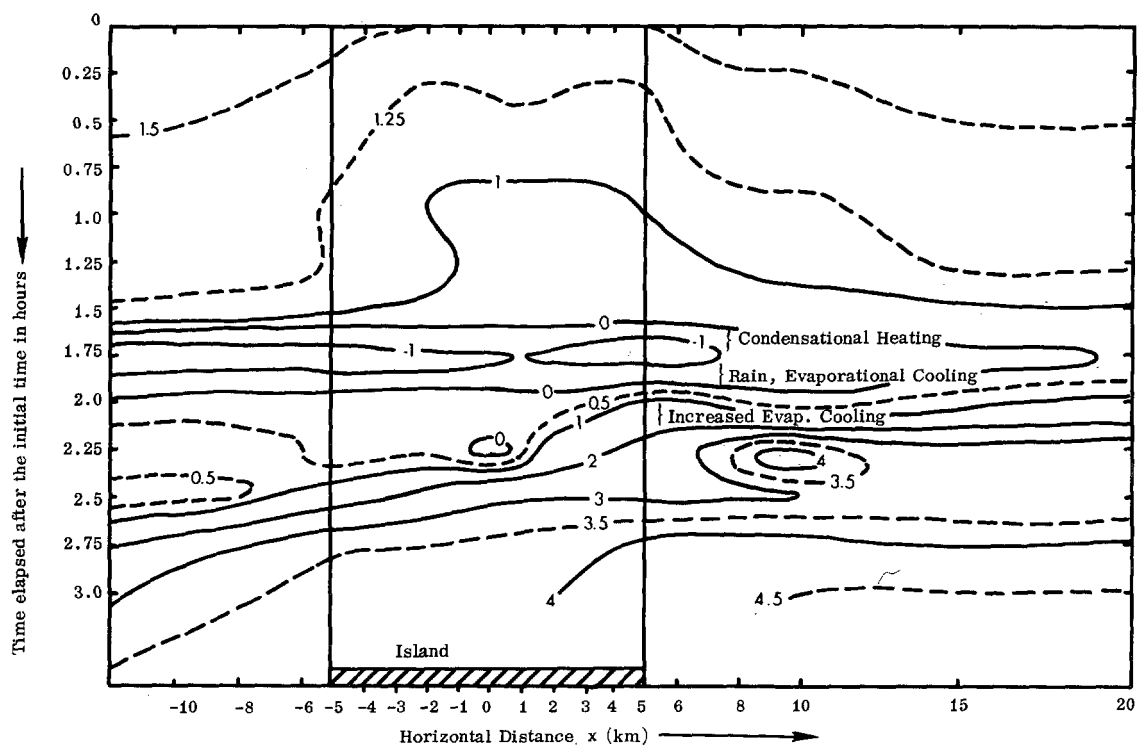
FIGURE 5.—The (x, t) cross section of surface pressure perturbation (mb).

The above features, together with the earlier discussions of the results, enable us to summarize the following predicted characteristics of the heated island phenomenon:

1. In the absence of large-scale disturbances, as on Aug. 27, 1970, the theoretical island, whose specifications correspond to the real Grand Bahama Island (GBI), does produce significant perturbations in the ambient atmospheric flow.

2. The leeward edge of the island is the preferred region for the initiation of perturbations.

3. The evaporational cooling of the ambient atmosphere by the falling rain forms a mesoscale High on the lee edge of the island. The resulting pressure distribution in turn sets up accelerations in the upwind direction and causes the propagation of the disturbance in that direction. That the evaporational cooling causes the upwind propagation is supported by the results of the dry model of Estoque and Bhumralkar (1969) in which no such feature was indicated in the absence of rain and evaporational cooling.

4. The life cycle of the disturbance induced by the theoretical heated island is approximately 2 to 2.5 hr.

Observational results. Figure 9 shows photographs made from individual frames of a time-lapse movie of clouds taken over GBI on the date under study. Below each photograph, we have indicated the local time at which it was taken. For proper orientation, it must be noted that the camera points toward the east; that is, along the longer axis of the island. The prevailing flow is from right to left across the photographs; this implies that, looking at the photograph, the leeward edge of the island is on the left and the upwind edge is on the right. The sequence of photographs shows the evolution of a disturbance through its complete life cycle. The prominent *observed* features evident on the basis of figure 9 are described in the following paragraphs. All times refer to local daylight time (EDT) at GBI.

As shown by the cloud photograph at 1350 EDT, there is

no significant weather activity over the island at this time. During the next 1 hr (1450 EDT) a disturbance develops to the leeward side of the island. In the ensuing ½ hr, this disturbance not only intensifies but also propagates in the upwind direction. This feature is shown clearly by the photograph at 1525 EDT, in which we can see well-organized cloudiness from the lee edge to the middle of the island in the upwind direction; also, the rain is reaching the surface. By 1625 EDT, the disturbance has intensified further and is spread over the entire width of the island; the photograph shows no clear skies, and it is raining all over. The conditions are shown to be generally undisturbed over the island at 1730 EDT; the disturbance has apparently completed its life cycle in 3–3½ hr.

On the basis of the above description and in conjunction with discussions of observations in Part I (Bhumralkar 1973, figs. 7–10), we see that there is reasonably good qualitative agreement between the model predictions and the observed atmospheric conditions of Aug. 27, 1970.

There are, however, certain discrepancies in the theoretical results and observations. The most notable is that our model predicts a shorter life cycle for the disturbance than is actually observed. It is our belief that this difference arises because our model tends to overestimate evaporational cooling, which in turn decreases the intensity of the pertubations. The model also predicts much higher bases for clouds than are observed in the vicinity of GBI. Both of these differences between theory and reality can be attributed to the use of a large constant value (200 m²/s) for the vertical diffusion coefficient. The use of this large coefficient value results in excessive drying of the atmosphere above the constant-flux layer since more moisture is diffused upward than is supplied from the surface through the constant-flux layer.
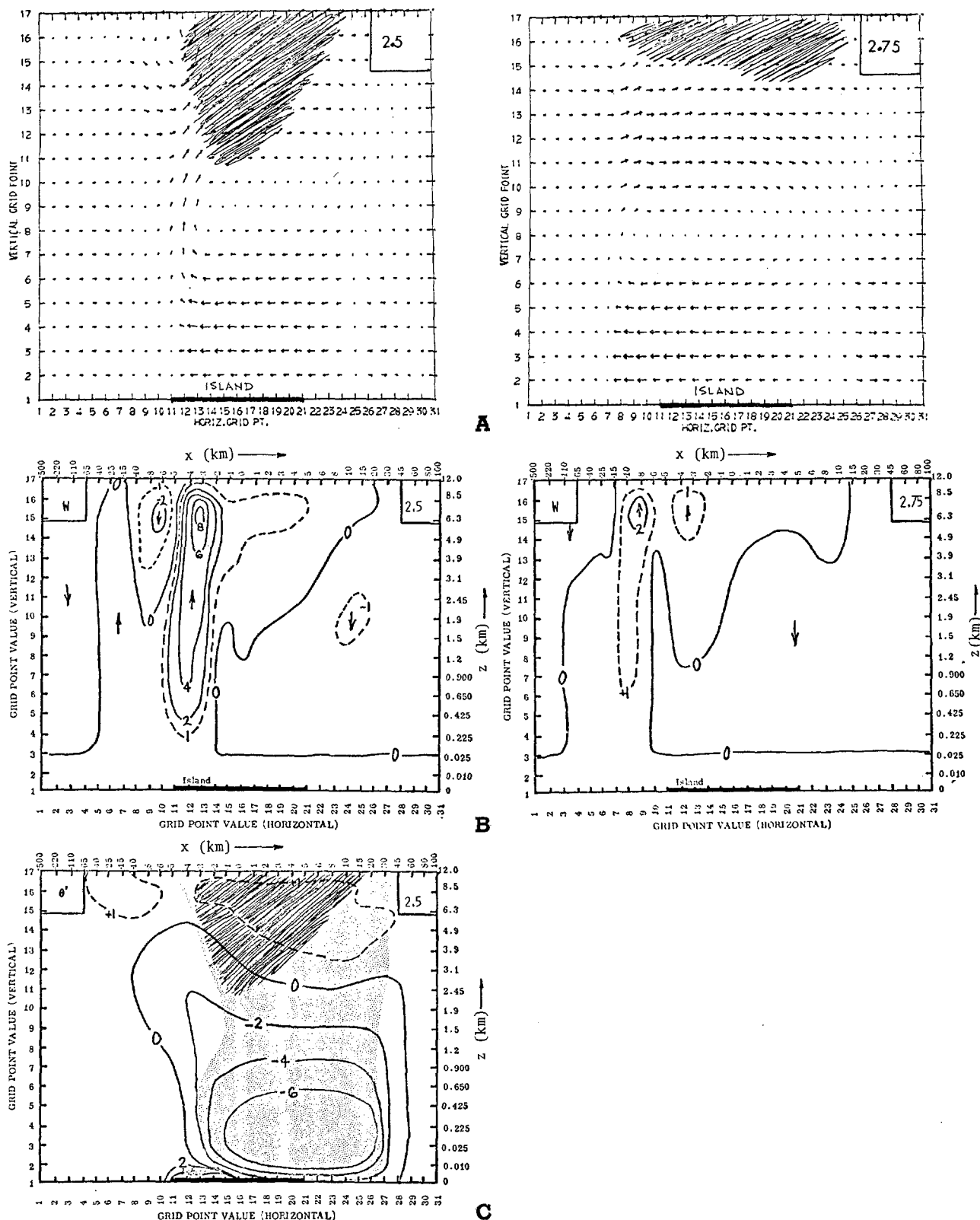
FIGURE 6.—Same as figure 2 for 2.5 and 2.75 hr.

Experiment 2: Influence of the Speed of the Prevailing Flow

Here, we present a comparison between the control experiment and experiment 2. This comparison provides another instance in which model predictions could be compared with observations (Bhumralkar 1973, figs. 12–15). We have selected the accumultaed precipitation at the surface as an index for comparing the results of experiments 1 and 2. As shown by the observations presented in Part I (Bhumralkar 1973, fig. 4), the prevailing conditions over the GBI are almost identical on Aug. 27 and Aug. 28, 1970. The only significant difference
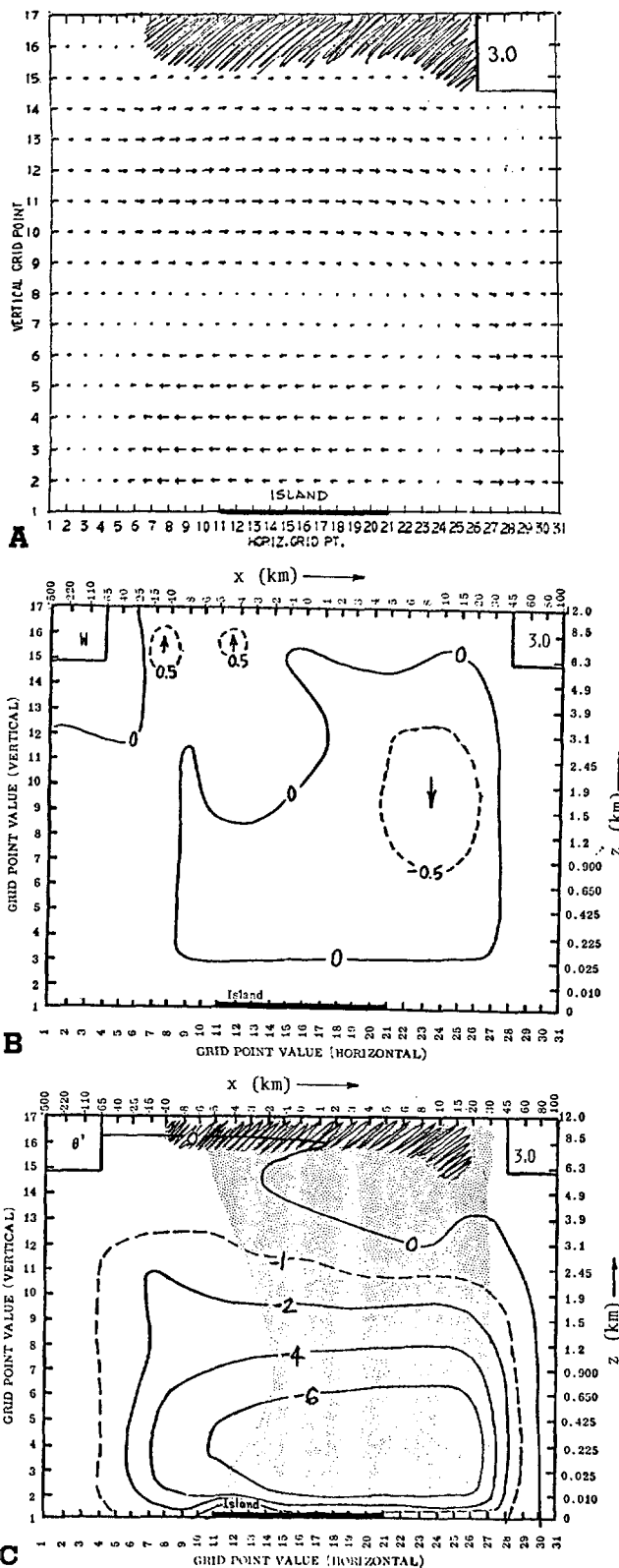
FIGURE 7.—Same as figure 2 for 3.0 hr.

shows the plot of cumulative rain at the surface after the model has been integrated for 3 hr of real time. Note that the strong wind speed of 12 m/s in experiment 2 prevents development of any significant perturbations. The influence of stronger wind in experiment 2 is also reflected in the location of the rainfall maximum 5 km downwind from the edge of the island. In this experiment, there was no release of latent heat and the maximum vertical velocity was 80 cm/s.

In *contrast*, the control experiment demonstrates that for almost identical conditions but weaker wind speed, a stronger disturbance is induced by the heated island. The rainfall maximum is only 1 km from the downwind edge, and the vertical motion reaches a maximum of 12 m/s after the release of latent heat of condensation. The difference in the magnitudes of vertical motions in these two experiments emphasizes the role of latent heat release in the intensity of the perturbation.

We explain the differences in the results of the control experiment and experiment 2 as follows:

Figure 11 shows the temperature perturbation fields for the control experiment (wind 155°/5 m/s) and experiment 2 (wind 155°/12 m/s). In the weaker wind case, the isotherms do not show any significant tilt in the downwind direction (fig. 11A). Also, during the half hour (from $t=1$ to 1.5 hr), the 1° isotherm moves through a distance of 2 km and does not extend beyond 2 km from the lee edge of the heated island. This suggests that the lowest pressure in the lower levels is located over the island and the configuration of isotherms maintains a relatively stronger pressure gradient close to the island. This results in formation of an updraft right over the island. When the wind is stronger (fig. 11B), the normal component causes shearing of isotherms in the downwind direction and, consequently, the isotherms show a distinct tilt. In this case, the 1° isotherm moves 15 km downwind from the lee edge of the island. The pressure gradient in this case is not as strong as in the weaker wind case.

Figure 12 shows a plot of temporal variations of the locations of updraft relative to the island. It is seen that in the weaker wind case the updraft, in response to the pressure distribution, stalls over the island itself. Consequently, due to its location over a source of buoyancy, the updraft intensifies and the release of latent heat of condensation causes further intensification of the disturbance. On the other hand, in the stronger wind case, the updraft moves downwind rapidly and reaches a location over the sea. Here, due to lack of a buoyancy source, the updraft weakens and there is no significant development of the disturbance over the island.

Results of Experiments 3 to 7

As stated earlier, model runs 3–7 have no observational support. We performed these experiments to analyze the behavior of the solutions of model equations by varying one factor at a time (table 2). The results of these experiments are compared with those of the control experiment by using the accumulated precipitation at the surface as an index for comparison.
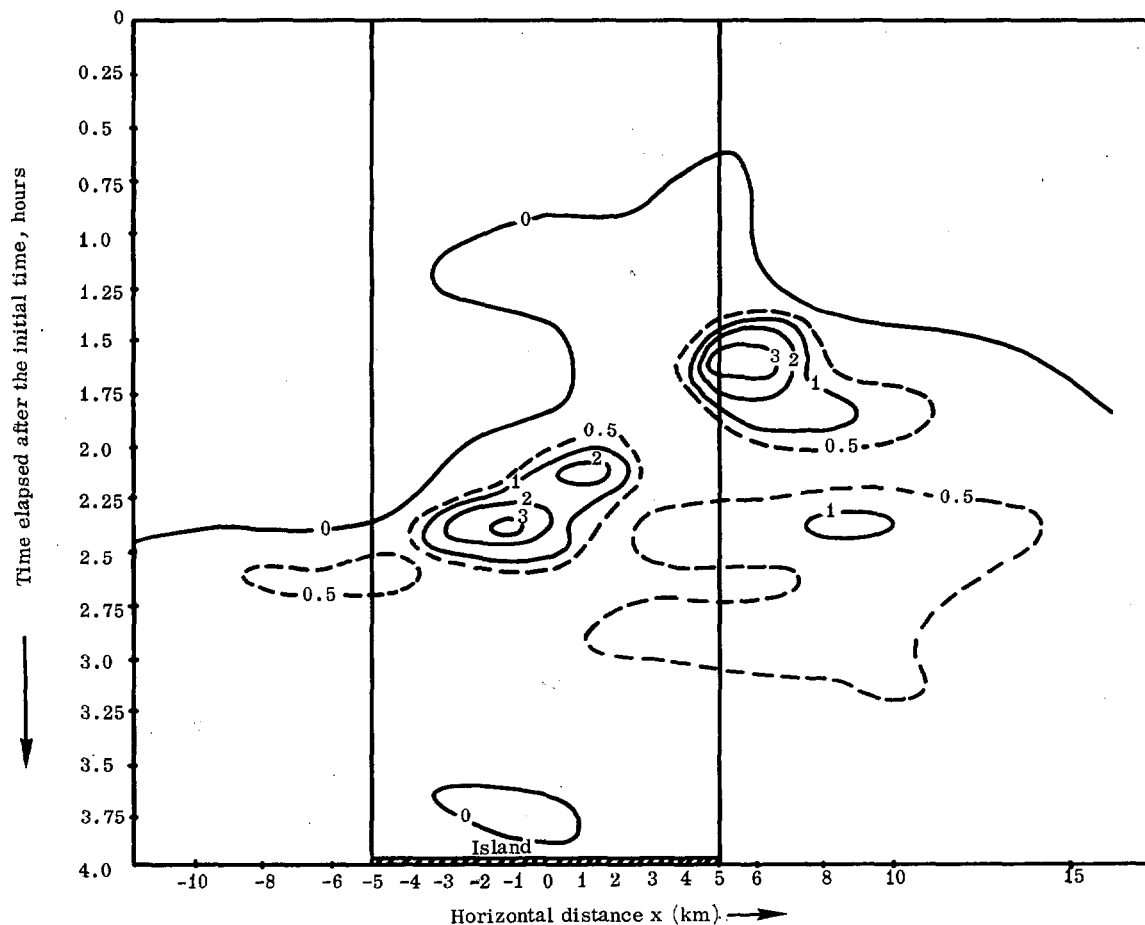
between these days is the speed of the prevailing flow; it is 5 m/s on August 27 and 12 m/s on August 28.

We integrate our model by prescribing the prevailing wind speed of 5 m/s for the control experiment and 12 m/s for experiment 2. Other initial conditions of temperature, moisture, and wind direction are the same. Figure 10

FIGURE 8.—The (x, t) cross section of rainfall rate at the surface (cm/15 min).

Experiments 3 and 4—Variations of $\Delta\theta$, the temperature excess of the heat source. The island surface temperature excess over its surroundings is the predominant driving force of the heated island circulations and, therefore, the most important parameter of the model.

For the control experiment, the island is 6°C warmer than the surrounding sea, whereas in experiments 3 and 4 it is warmer by 9° and 3°C, respectively. A plot of cumulative rainfall at the surface for all three experiments is shown in figure 13. As expected, the intensity of perturbations is the greatest for $\Delta\theta=9$°C. In experiment 4 ($\Delta\theta=$ 3°C), there is no rainfall at all. In the case of greater $\Delta\theta$, the air over the island is more buoyant; also, the stronger pressure gradients tend to bring a greater supply of moisture from over the sea into this more buoyant air over the island. These factors contribute to greater intensity of perturbations and rainfall.

Experiment 5—Influence of the variation in the parallel component of the wind. This comparison brings out the effect of the magnitude of the wind component, v, parallel to the heated island. Whereas the normal component, u, is the same in the two experiments, v is 4.6 m/s in the control experiment and 10 m/s in experiment 5. Figure 14 shows a comparison between the two cases.

Note that the intensity of the perturbation is more pronounced when the v component is stronger. This result

is similar to the case in which temperature excess of the island is increased from 6° to 9°C. Figure 15 shows a comparison between the control experiment ($v=4.6$ m/s, $\Delta\theta=6$°), experiment 3 ($v=4.6$ m/s, $\Delta\theta=9$°), and experiment 5 ($v=10$ m/s, $\Delta\theta=6$°).

We see that the effect of increasing the magnitude of the v component produces the same effect (but not as intense) as that produced by increasing $\Delta\theta$ from 6° to 9°C. This correspondence in the curves for experiments 3 and 5 leads us to suggest that if the component of wind parallel to the island increases, it tends to cause greater mixing of heat, which in turn causes more intense disturbances. It may be remarked here that the increased frictional convergence due to the increase in the parallel component of wind also contributes towards development of stronger perturbations. However, this factor is relatively more important than the heat flux effect *only* during the initial stages when the vertical velocity is not strong enough to release the instability.

The results for experiment 5 also demonstrate the sensitivity of the intensity of the disturbance to the normal component of wind. Actually, if the normal component vanishes, then the perturbation would occupy a central position on the island (Estoque and Bhumralkar 1969). Observations have also shown that when the prevailing flow is down the longer axis of the heat source,
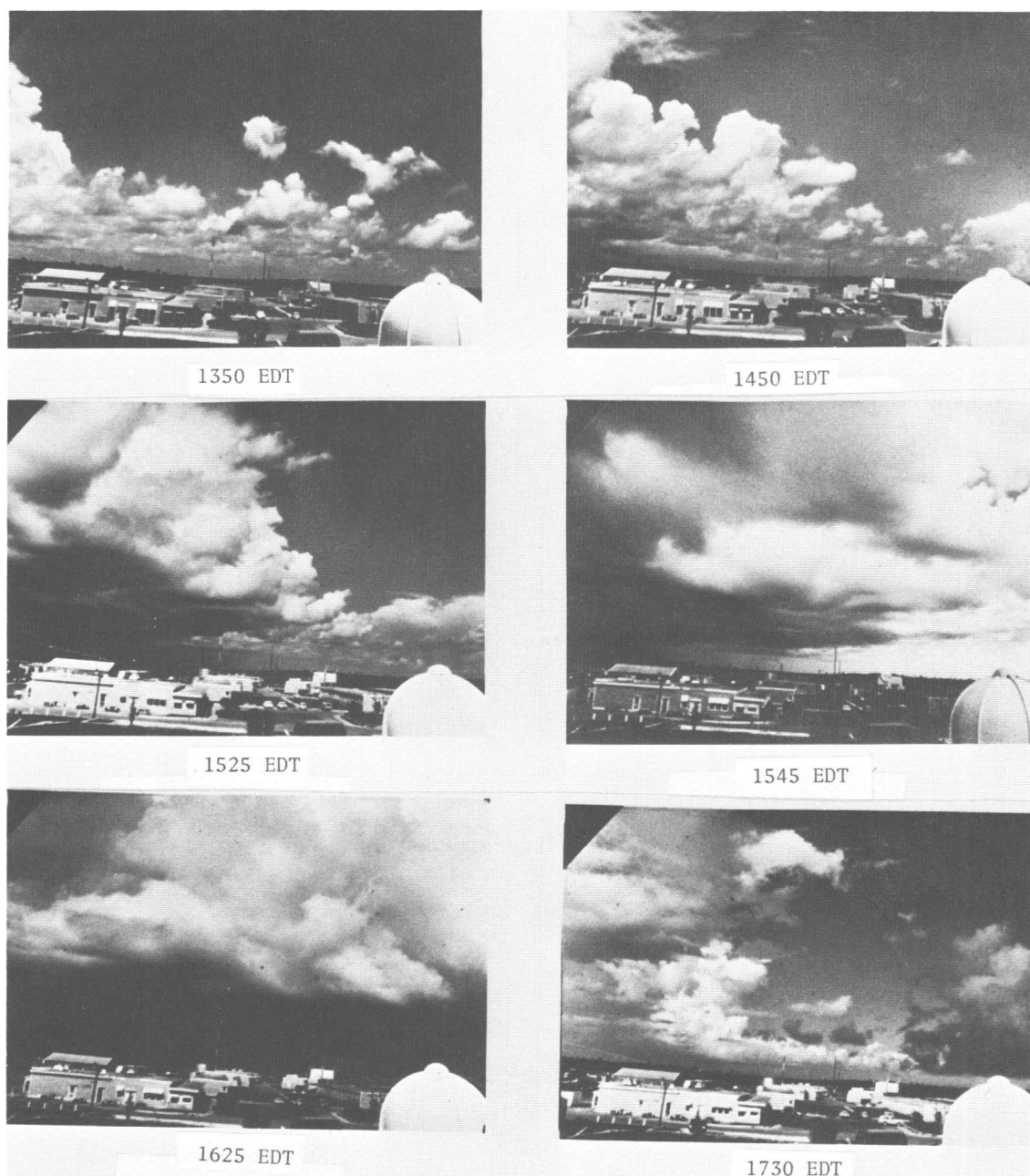
FIGURE 9.—Photographs showing evolution of cloudiness associated with the disturbance induced by Grand Bahama Island.
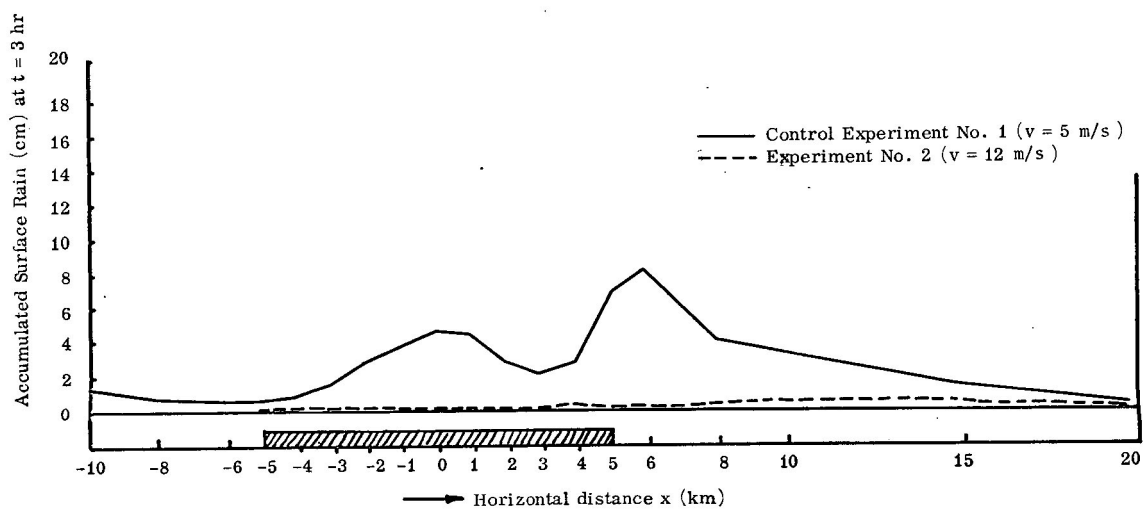

FIGURE 10.—Dependence of surface rainfall on the speed of the prevailing flow.
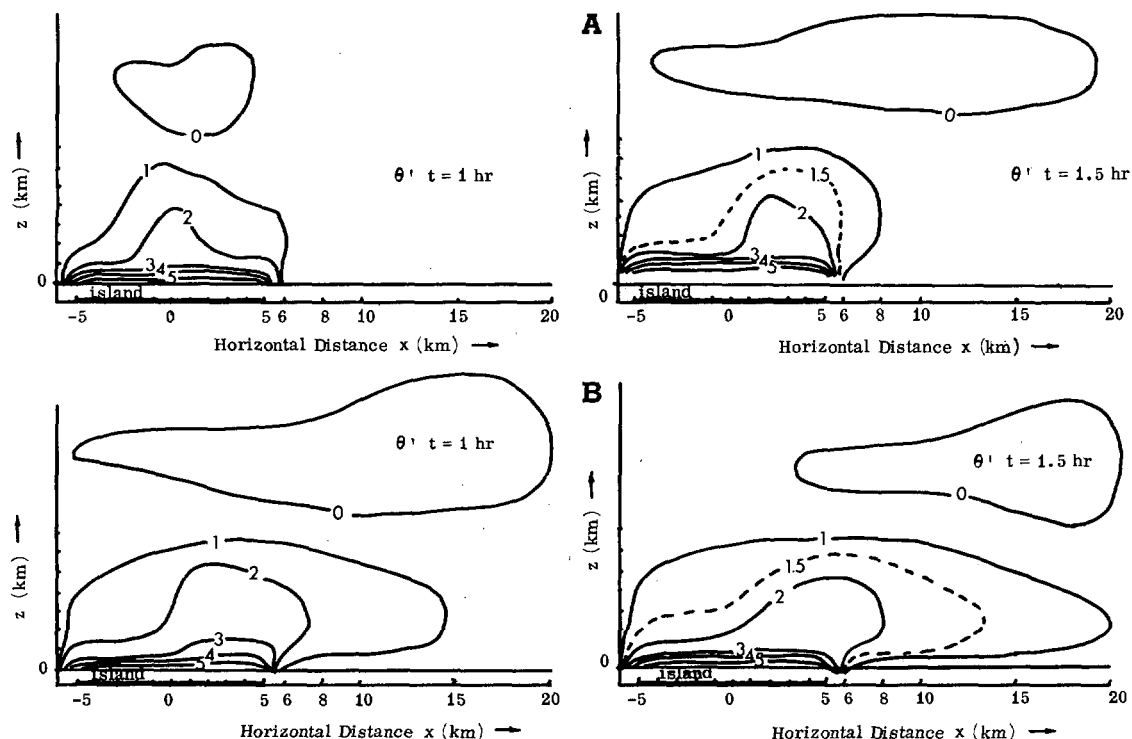
FIGURE 11.—Perturbation potential temperature (°C) fields for (A) the control experiment (wind 155°/5 m/s) and (B) experiment 2 (wind 155°/12 m/s).

that is, when there is *no* normal component, a single convective cell tends to develop more or less equidistant from the coast line (Lavoie 1968).

Experiments 6 and 7—Influence of the width (L) of the heated island. Here, we discuss the influence of the width of the heated island on the induced perturbations. For the control esperiment, the island is 10 km wide; in experiments 6 and 7, the width is 4 km and 2 km, respectively. Figure 16 shows a comparison of these three experiments. We can see that in the cases of smaller width (experiments 6 and 7) there is only one peak in rainfall; in the control experiment ($L=10$ km) there is a double maxima. In all three cases, the maximum is located downwind of the island at a distance of 1–2 km from the edge. This confirms our earlier result that the leeward edge is the preferred region for the formation of strong perturbations. The most important inference that can be drawn from this set of experiments is that, under favorable conditions of the prevailing flow, an island as small as 2 km wide can also produce rainfall. This has an important bearing on the feasibility of producing rain artificially by asphalt ground coatings (Black 1963).

8. CONCLUSIONS

Our theoretical model was developed in conjunction with a specially designed field program with a view to testing the correspondence between the predictions of the model and actual observations. From our experience, the importance of such a dual approach in theoretical research cannot be overemphasized. Our model has demonstrated a significant skill in simulating the general mesoscale
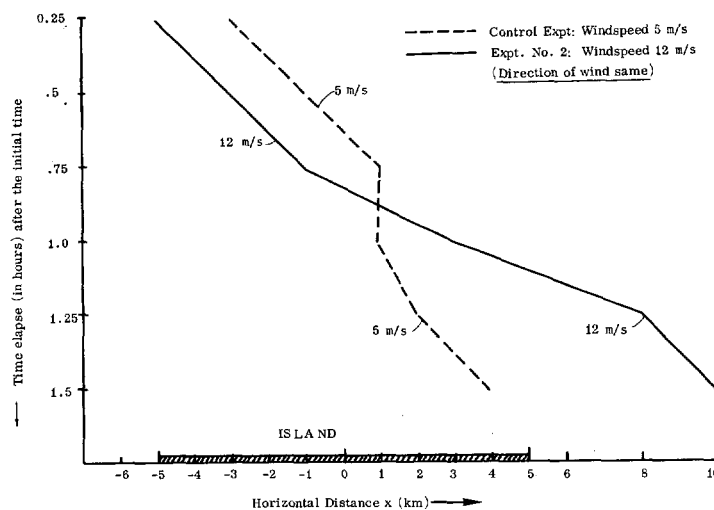

FIGURE 12.—Time variations of the location of updraft as a function of wind speed.

characteristics of disturbances induced by the heated island (Grand Bahama Island). The degree of correspondence with reality, though only qualitative, suggests that the model perhaps provides a useful means for predicting the alterations in the airflow structure and cloud and rain distributions caused by a localized heat source. There is reason to believe that the basic modeling approach introduced here could be applied to a variety of meteorological problems dealing with heat sources at the surface. The model, with a few modifications, can also be used for predicting quantitatively the dispersion of air pollutants by mesoscale circulations. The model can also handle problems dealing with weather modification induced by
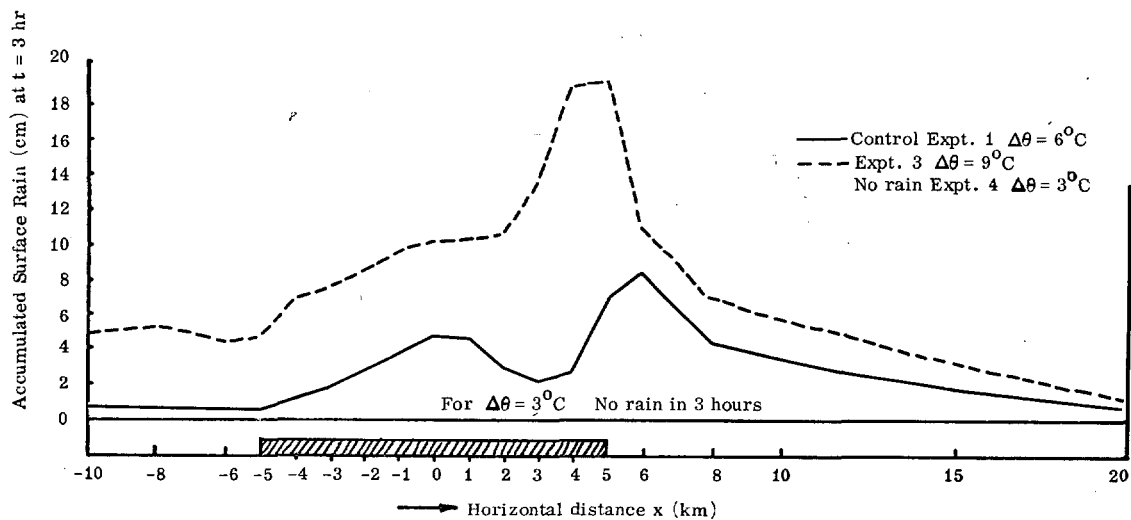
FIGURE 13.—Influence of temperature excess, $\Delta\theta$, of the island on the surface rain.
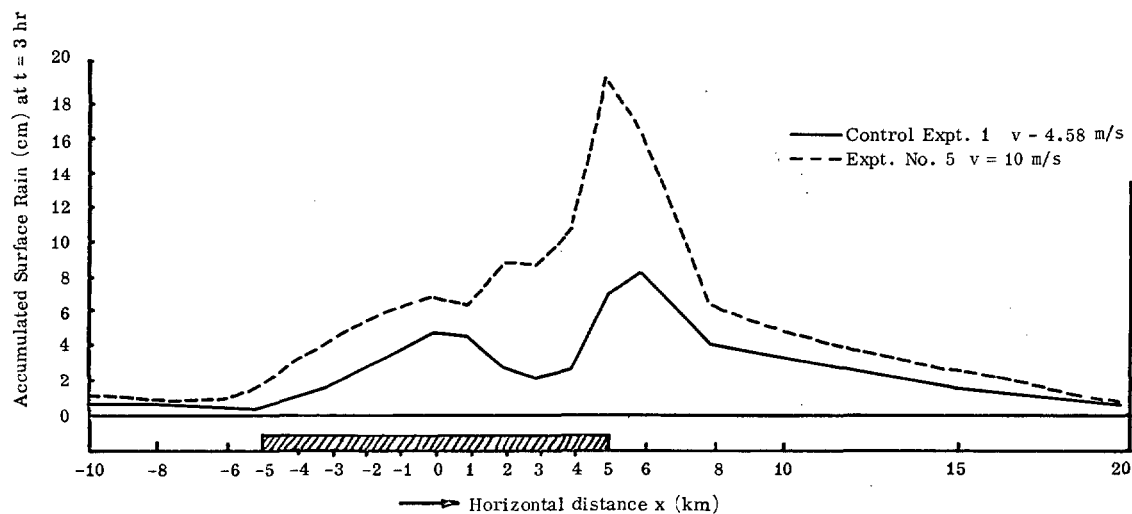

FIGURE 14.—Influence of the strength of the wind component, v, parallel to the island, on the surface rain.
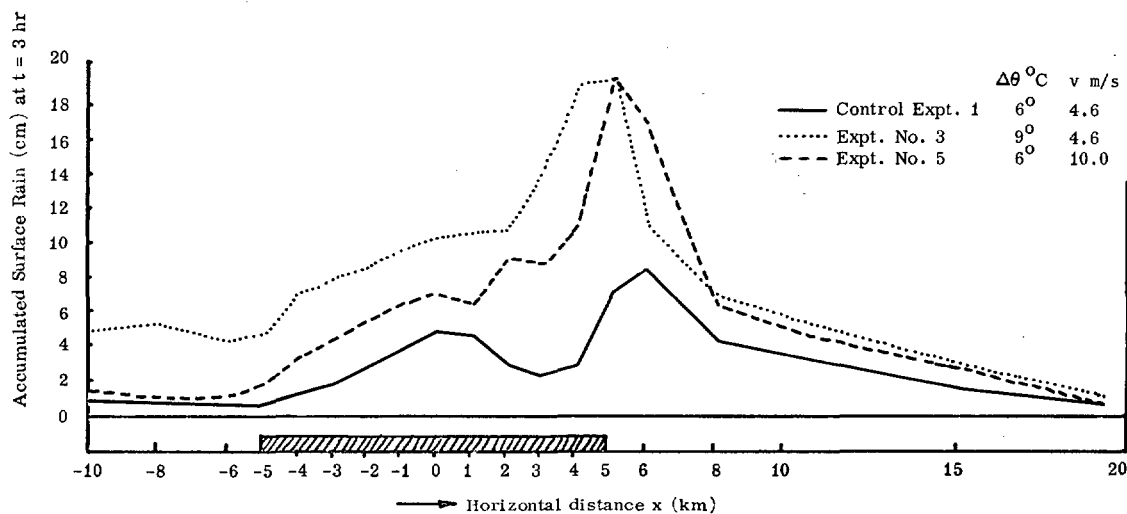

FIGURE 15.—Plot showing comparison between the influence of temperature excess of the island and parallel component of the wind.
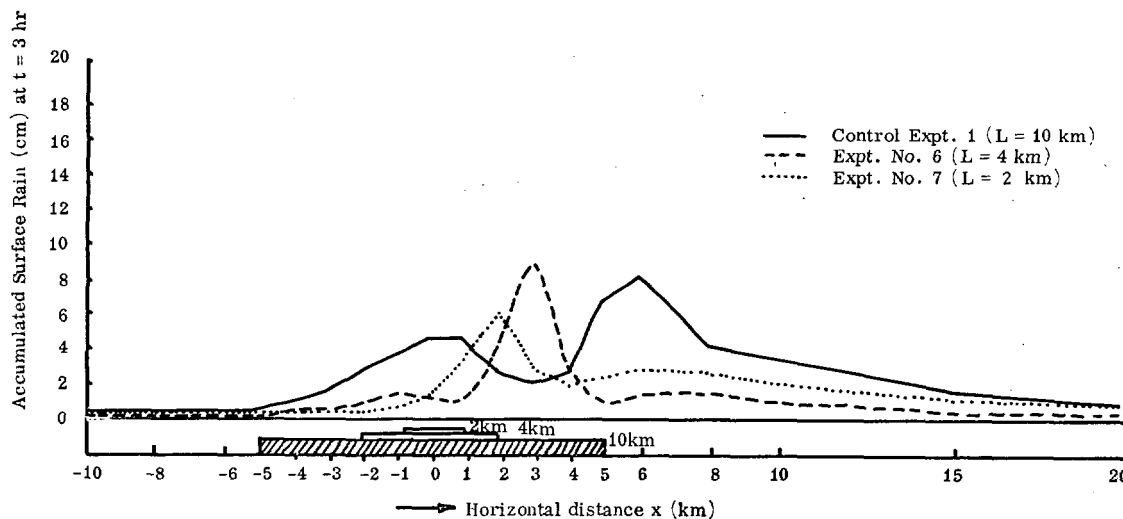
FIGURE 16.—Influence of the width (L) of the island on surface rain.

asphalt coatings insofar as it concerns the feasibility of producing rain artificially. Thus, the model has immense possibilities at least as a research tool and maybe as a local forecast tool under certain conditions.

9. SUGGESTIONS FOR FURTHER RESEARCH

The following refinements appear desirable to improve the usefulness of the approach described here.

1. The model should include the ice phase, since severe mesoscale disturbances are generally accompanied by the formation of ice.

2. One may wish to treat diffusion processes more realistically by experimenting with nonlinear diffusion coefficients used by Smagorinsky (1963) and others.

3. The numerical intergration of the model should be performed by using energy-conserving higher order schemes instead of the forward-upstream scheme, which is of first order only.

4. Since most natural surface inhomogeneities are irregular, the vertical cross-section models do not treat the local weather problems associated with urban heat islands, lakes, and coastal regions adequately. Therefore, it is suggested that the models may be extended to include the third space dimension.

5. The hydrostatic assumption should be eliminated.

6. The role of shear should be analyzed in detail.

REFERENCES

Bhumralkar, C. M., "An Observational and Theoretical Study of Atmospheric Flow Over a Heated Island," *Final Report*, National Science Foundation Grant No. GA–14156, University of Miami, Coral Gables, Fla., Mar. 1972, 150 pp.

Bhumralkar, C. M., "An Observational and Theoretical Study of Atmospheric Flow Over a Heated Island: Part I," *Monthly Weather Review*, Vol. 101, No. 10, Oct. 1973, pp. 719–730

Bhumralkar, C. M., "Effect of Moisture on the Hydrostatic Pressure," *Journal of Applied Meteorology*, Vol. 13, No. 1, Feb. 1974 (in press).

Black, J. F., "Weather Control: Use of Asphalt Coatings to Tap Solar Energy," *Science*, Vol. 139, No. 3551, Jan. 1963, pp. 226–227.

Estoque, M. A., "Vertical Mixing Due to Penetrative Convection," *Journal of the Atmospheric Sciences*, Vol. 25, No. 6, Nov. 1968, pp. 1046–1051.

Estoque, M. A., and Bhumralkar, C. M., "Flow Over a Localized Heat Source," *Monthly Weather Review*, Vol. 97, No. 12, Dec. 1969, pp. 850–859.

Kessler, Edwin, "On the Distribution and Continuity of Water Substance in Atmospheric Circulation," *Meteorological Monographs*, Vol. 10, No. 32, American Meteorological Society, Boston, Mass., Nov. 1969, 84 pp.

Lavoie, Ronald L., "A Mesoscale Numerical Model and Lake-Effect Storms," Ph.D. dissertation, The Pennsylvania State University, University Park, 1968, 102 pp.

Orville, Harold D., and Sloan, Lansing J., "A Numerical Simulation of the Life History of a Rainstorm," *Journal of the Atmospheric Sciences*, Vol. 27, No. 8, Nov. 1970, pp. 1148–1159.

Richtmyer, R. D., "Difference Methods for Initial Value Problems," Interscience Publishers, New York, N.Y., 1957, 238 pp.

Smagorinsky, Joseph, "General Circulation Experiments With the Primitive Equations: I. The Basic Concept," *Monthly Weather Review*, Vol. 91, No. 3, Mar. 1963, pp. 99–165.

Sutton, O. G., "Micrometeorology: A Study of Physical Processes in the Lowest Layers of the Earth's Atmosphere," McGraw-Hill, New York, N. Y., 1953, 333 pp.

Takeda, Takao, "Numerical Simulation of a Precipitating Convective Cloud: The Formation of a 'Long-Lasting' Cloud," *Journal of the Atmospheric Sciences*, Vol. 28, No. 3, Apr. 1971, pp. 350–376.